Effect of laser-shock peening on the structure and nano-mechanical behavior of a Ti-based metallic glass

Yang Lv[1], Wei Yue[1], Zheng Cao[1], Hongbo Fan[2], Zhiliang Ning[1*], Jianfei Sun[1], Peter K. Liaw [3], and Yongjiang Huang[1*]

[1] National Key Laboratory for Precision Hot Processing of Metals, Harbin Institute of Technology, Harbin 150001, China

[2] Space Environment Simulation Research Infrastructure, Harbin Institute of Technology, Harbin 150001, China

[3] Department of Materials Science and Engineering, University of Tennessee, Knoxville, USA

[*] Corresponding author: yjhuang@hit.edu.cn (Y.J. Huang); zhiliangning@sina.com (Z.L. Ning)

Abstract

As a versatile and nondestructive method, laser-shock peening (LSP) has been extensively utilized to improve the mechanical properties of metallic components. Nevertheless, the underlying mechanism for the LSP-induced amorphous structure transformation remains unclear. In this study, the structure and nano-mechanical properties of a $Ti_{40}Zr_{25}Ni_3Cu_{12}Be_{20}$ bulk metallic glass (BMG) were investigated before and after LSP processing. The LSP-treated BMG sample remains as an amorphous structure. A higher laser-beam energy causes a lower local order level, a higher free volume content, a greater shear-band density for the studied BMG samples, causing a lower nano-hardness. There exists a gradient in nano-hardness along the LSP direction inside the sample, which can be attributed to the gradual decay of the shock-wave pressure with increasing the depth.

Keywords: Metallic glass, Laser-shock peening, Free volume, Shear bands, Nano-hardness

1. Introduction

Due to the unique atomic configuration of long-range disorder and short-range order, bulk metallic glasses (BMGs) often offer many outstanding properties, such as the high yield strength, excellent corrosion and fatigue resistance properties, compared with traditional crystalline materials [1-8]. Nevertheless, the plastic flow of BMGs usually localized within nano-scaled narrow regions, resulting in low plasticity and catastrophic fracture under tensile loading, which severely restricts their applications in engineering [9, 10]. To overcome this limitation, external mechanical processing is actively applied [11-20]. Among them, shot peening and cold rolling have been proven to be effective in improving mechanical properties of BMGs. As a versatile and nondestructive surface-treatment method, laser-shock peening (LSP) can be used to finely tune mechanical properties of materials [14, 15, 18, 21-24]. During LSP, the laser pulse with a high energy density (GW/cm^2) and extremely short duration (ns) propagates from the surface into the materials, generating great residual stresses and multiple shear bands on the sample surface, and thus favoring their enhanced mechanical performance [11]. Nowadays, LSP has been considered as an appropriate method to improve the plasticity of monolithic BMGs. Mahmoud et al. [15] applied LSP to $Zr_{35}Ti_{30}Cu_{10}Ni_5Be_{20}$ BMGs, and revealed that LSP had a great impact on the structure along the depth direction, and strong variation in the surface structural heterogeneity induced by LSP rendered the structure "younger" (with a higher free volume content). Zhang et al. [11] and Cao et al. [22] treated the $Zr_{41.25}Ti_{13.75}Ni_{10}Cu_{12.5}Be_{22.5}$ BMG by LSP and attributed its enhanced plasticity to the introduce of compressive residual stress. Zhu et al. [25] observed a micro-indent on the surface of LSP-treated $Zr_{41.2}Ti_{13.8}Cu_{10}Ni_{12.5}Be_{22.5}$ BMGs, and ascribed its surface softening to the high-density shear bands. However, the underlying mechanism of the evolution in the structures and mechanical properties of

BMGs induced by LSP remains unclear.

This study focuses on how the introduction of LSP affects the structures and mechanical properties of a Ti-based BMG. The effect of laser-beam energies on the flow unit, free volume, shear transformation zones (STZs), and shear bands of the studied BMG samples will be elucidated. Additionally, the reasons for nano-hardness changes induced by LSP will be carefully interpreted. The results will help us further understand the effects of LSP on the structures and mechanical properties of BMGs.

2. Experimental details

The alloy ingots with a chemical composition of $Ti_{40}Zr_{25}Ni_3Cu_{12}Be_{20}$ (at. %) were fabricated via arc melting mixtures of Ti, Zr, Ni, Cu, and Be metals [99.5 ~ 99.99 weight percent (wt.%) purity] in a Ti-gettered argon atmosphere. To ensure chemical composition homogeneity, the ingots were re-melted at least five times with electromagnetic stirring. Then the alloy melts were cast into a copper mold. The resulting sample has a dimension of 3 mm×30 mm×70 mm. Subsequently, plate-shaped samples with a dimension of 1 mm × 6 mm×6 mm were electric-discharge machined from the cast sample, and carefully polished with SiC abrasive papers to a mirror finish. After then, the LSP treatment is employed on the BMGs sample surfaces, as illustrated in Fig. 1(a). For LSP processing, an aluminum foil of a 0.1-mm thickness, and a water layer of 1-mm thickness were used as an absorption layer, and a constraint layer, respectively. The LSP parameters are listed as follows: a wavelength of 1,064 nm, pulse width of 15 ns, laser spot diameter of 3.8 mm, and overlap rate of 50 %. Additionally, the laser beam scans along a zigzag path. Three laser beam energies of 8J, 13J, and 18J are selected, and the as-cast and LSP-treated BMG samples at different energies are shown in Fig. 1(b). A three-dimensional solid element of 6 mm × 6 mm × 1 mm (length × width × thickness) was constructed by the ABAQUS software with a precise mesh, and the residual stress induced by LSP in the BMGs along the depth direction was examined by a finite element simulation method.

X-ray diffraction (XRD, D8-ADVANCE) with Cu Kα radiation, scanning electron

microscopy (SEM, Merlin Compact) equipped with an energy-dispersive X-ray spectroscopy (EDS), and transmission electron microscopy (TEM, FEI Talos f200x) operated at 200 kV were used to characterize the structures of the studied BMG samples before and after the LSP treatment. The high-resolution TEM (HRTEM) images [26] were obtained to reveal the atomic-level structures of BMG samples, and the images were transformed using an auto-correlation function (ACF) to analyze the change in local order. A series of room-temperature nanoindentation tests were performed on as-cast and LSP-treated samples along the depth direction using a nanoindentation instrument (Agilent G200) equipped with a Berkovich diamond indenter (radius of 20 nm under a displacement-controlled mode, with a displacement rate of 10 nm/s, a maximum depth of 200 nm, and a holding time of 5 s at maximum depth). To ensure reliability, at least five tests were conducted at each sample condition. Finally, the morphologies of nanoindentation remarks were examined by SEM.

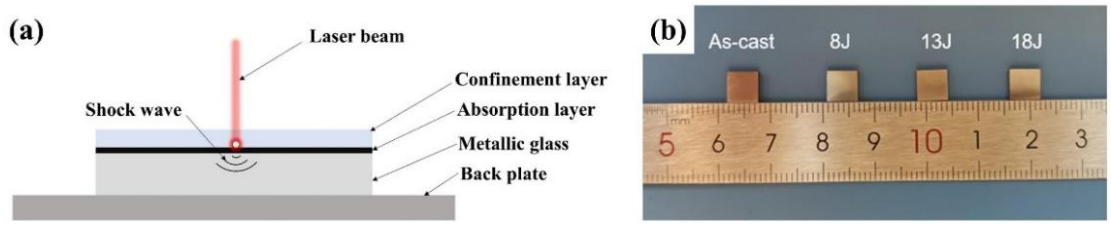

Fig. 1. (a) Schematic of the LSP treatment and (b) the image of as-cast and LSP-treated $Ti_{40}Zr_{25}Ni_3Cu_{12}Be_{20}$ bulk metallic glass samples with different laser beam energies (8J, 13J, and 18J).

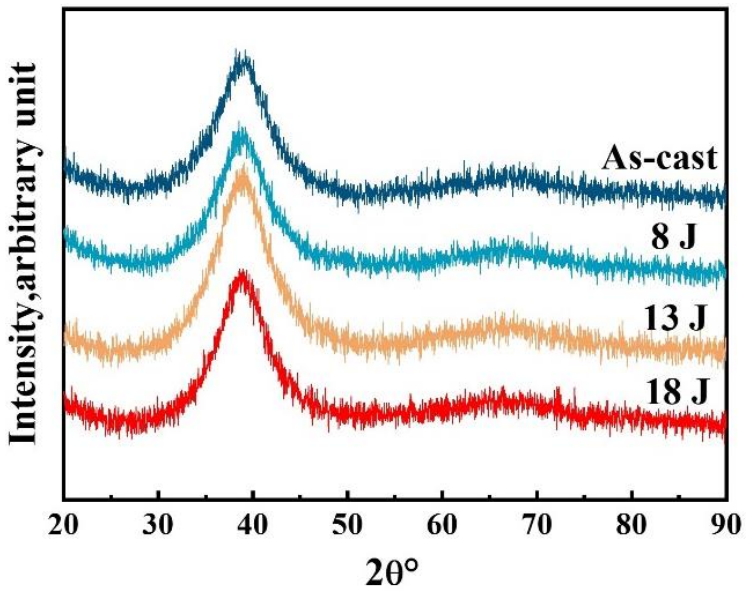

Fig. 2. XRD patterns of as-cast and LSP-treated $Ti_{40}Zr_{25}Ni_3Cu_{12}Be_{20}$ bulk metallic glass samples with different laser beam energies.

3. Results and discussion

Figure 2 shows the XRD patterns of the as-cast and LSP-treated samples with different laser beam energies (8J, 13J, and 18J). As can be seen, besides only a broad diffusing maximum at about 40°, no distinct Bragg peaks corresponding to crystalline phases can be detected for all the samples. This feature reveals that the studied Ti-based BMGs sample retains its glassy structure after LSP processing.

During LSP, the laser pulse vaporizes the absorption layer on the material surface into a high-pressure plasma, and the rapid expansion of the plasma generates a high-pressure shock wave that diffuses onto the matrix. When the peak pressure of the shock wave surpasses the elastic limit, the material undergoes plastic deformation, generating compressive residual stresses on the matrix surface [11, 27]. Furthermore, the shock wave pressure produced on the matrix surface is proportionate to the LSP energy. For the purpose of simulating the residual stress in BMGs affected region, a three-dimensional (3D) solid element of 6 mm × 6 mm ×1 mm (length × width × thickness) is established by ABAQUS software and accurately meshed. Base on the Fabbro's shock wave model [28], the maximum pressure produced by a laser beam in the constrained structure, P_{max}, is determined, as depicted in the following formula:

$$P_{max} = 10^{-9}\left(\frac{\alpha}{2\alpha+3}\right)^{1/2} Z^{1/2} {I_0}^{1/2} \quad (1)$$

where $Z = 2/(1/Z_1 + 1/Z_2)$ is the equivalent acoustic impedance, Z_1 and Z_2 are the acoustic impedance of BMGs and confined the water layer, respectively. In the present work, the value of the acoustic impedance of BMGs and confined the water layer are 1.29×10^7 kg/m^2·s. I_0 is the laser-power density, which can be determined as follows:

$$I_0 = \frac{4E}{\pi d^2 \tau} \quad (3)$$

where E is the laser-beam energy, d is the laser-beam diameter, and τ is the pulse width. P_{max} corresponding to the energies of 8J, 13J, and 18J are calculated to be 2.76 GPa, 3.52 GPa, and 4.14 GPa, respectively.

Taking the Gaussian distribution and the two-dimensional shock wave pressure induced by the laser-beam irradiation into account, the following equation can be applied [29],

$$P(r,t) = P(t)exp\left(\frac{r^2}{2R^2}\right) \quad (4)$$

where R and r are the radius of the laser beam and radial distance from the laser beam center, respectively. In this experiment, the value of R is 1.9 mm, and the value of r is less than or equal to R.

The simulation results are exhibited in Fig. 3. As shown in Figs. 3(a)-3(c), a residual stress is generated in the LSP-treated samples surface, and the distribution of the surface-residual stress is closely related with the laser-beam energy. To obtain a specific variation in surface residual stresses, Figure 3(d) displays the quantitative analysis of simulation results. As seen, the residual stresses at a depth less than 250 μm are compressive stresses, and the stress value increases with increasing the applied laser-beam energy. When the depth exceeds 250 μm, the residual stress changes from the compressive to tensile stress. As the depth further increases, the residual compressive and tensile stresses alternate. Finally, the stress progressively approaches 0 MPa for all the applied laser-beam energies. The variation of residual stresses indicates that the LSP-treated sample surface suffers a certain plastic deformation, and the extent of deformation is positively correlated with the applied laser-beam energy.

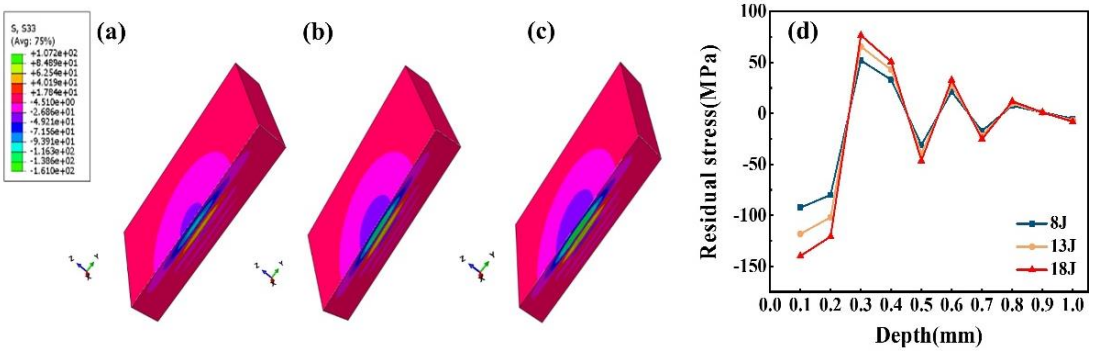

Fig. 3. Residual-stress distribution of $Ti_{40}Zr_{25}Ni_3Cu_{12}Be_{20}$ bulk metallic-glass samples with

different laser beam energies

(a) 8J, (b) 13J, (c) 18J, and (d) stress variation.

When the laser pulse impacts the BMG surface, the shock wave lowers the energy barrier in the system, making it easier for the flow unit to activate [30]. Numerous activated flow units begin to extend and coalesce, ultimately leading to BMG yielding [31, 32]. The plastic deformation of a BMG is well-known to take place via STZs [33]. Besides, the activation of STZs is closely related to the initial free-volume content. To further elucidate the structural evolution of the studied BMG during LSP, the local ordering is quantitatively examined in the present study. The ACF analysis is performed on the HRTEM image of the samples [26]. The HRTEM images [See Fig. 4(a)-4(g)] were divided into 64 sub-images with a size of 2.125×2.125 nm^2, which is comparable to the size of a medium-range-order atomic cluster. Each image is processed by the fast-Fourier-transformation (FFT), and the sub-images with crystal-like diffraction spots are selected as a reference to calculate the local order extent. Finally, the local order levels in the studied BMG before and after LSP processing are obtained by statistically calculating the ratio of ordered sub-images relative to the total amount of sub-images. A lower local order extent signifies a significant volume difference between ideal and actual amorphous structures, corresponding to a higher free-volume content. The local order extents are 9.38 %, 6.25 %, 4.69 %, and 3.16 % in as-cast and LSP-treated (8J, 13J and 18J) samples, respectively [as shown in Figs. 4(b)-4(h)]. Compared to the as-cast sample, LSP-treated samples exhibit lower local order extents. Furthermore, a higher laser-beam energy produces a more intense shock wave, which reduces the local order extent further. Such a condition increases the probability of atoms deviation from the perfect close-packed structure. Consequently, the density of the activated flow unit and free-volume content increase.

To further explore the effect of LSP on the nano-mechanical properties of the studied BMG, the morphologies of nanoindentation impressions of the samples are observed, using SEM, and the corresponding SEM images are shown in Fig. 5. For the as-cast

BMG sample, no significant differences can be found in its indentation morphologies at various depths, i.e., different distances from the sample surface along the LSP direction [See Figs. 5(a)-5(c)]. Nevertheless, there are pile-ups formed around the indentation by semicircular shear bands, as indicated by the yellow arrow [Figs. 5(d)-5(f), 5(g)-5(i) and 5(j)-5(l)]. During the penetration of a Berkovich diamond indenter into the surface of the studied BMGs, the region near the indenter undergoes softening under the supply of high stresses. Under the constraint of the undeformed regions and indenter, the softened regions accumulate upward, favoring the formation of pile-ups [34]. As the applied laser-beam energy increases from 8J [Fig. 5(d)] to 18J [Fig. 5(j)], more pile-ups form on the sample surface, suggesting more shear bands. Meanwhile, an increase in the depth [i.e., the distance from the sample surface along LSP direction] causes a decrease in the quantity of shear bands. In a word, as the shock-wave pressure increases, a free-volume content of $Ti_{40}Zr_{25}Ni_3Cu_{12}Be_{20}$ BMGs samples increases. A higher free-volume content further promotes the formation of more STZs inside the studied samples. Therefore, the activation and rearrangement of more STZs forms more shear bands, which is consistent with the above results (See Fig. 5).

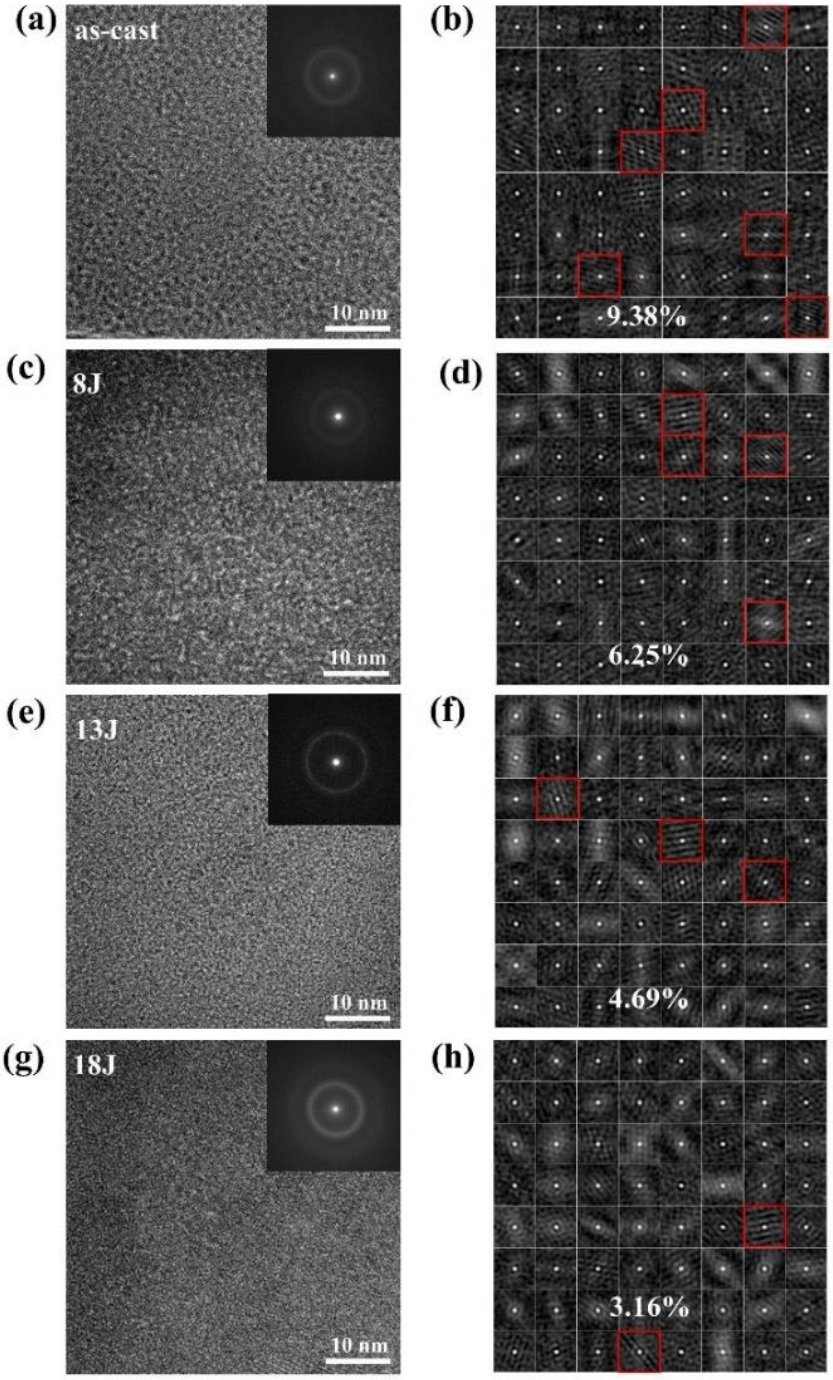

Fig. 4. HRTEM images with an inset show the selected area electron diffraction pattern (left), and the corresponding ACF images (right) of LSP-treated $Ti_{40}Zr_{25}Ni_3Cu_{12}Be_{20}$ bulk metallic glass samples with different laser-beam energies:(a) (b) as-cast, (c) (d) 8J, (e) (f) 13J, and (g) (h) 18J.

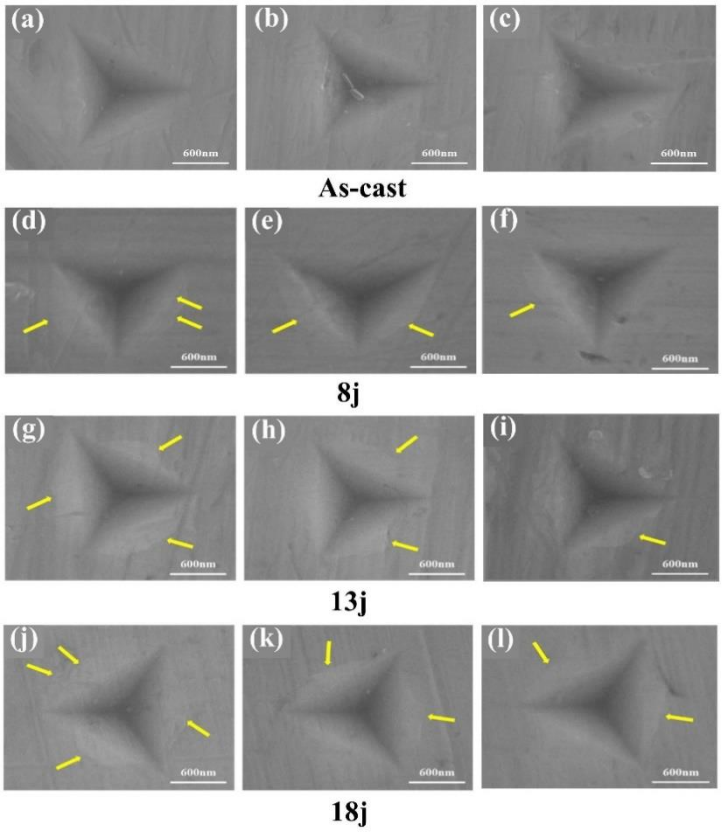

Fig. 5. Nanoindentation morphologies at different depths of as-cast and LSP-treated $Ti_{40}Zr_{25}Ni_3Cu_{12}Be_{20}$ bulk metallic glass samples with different laser-beam energies: (a) (d) (g) (j) 100 μm, (b) (e) (h) (k) 200 μm, and (c) (f) (i) (l) 300 μm.

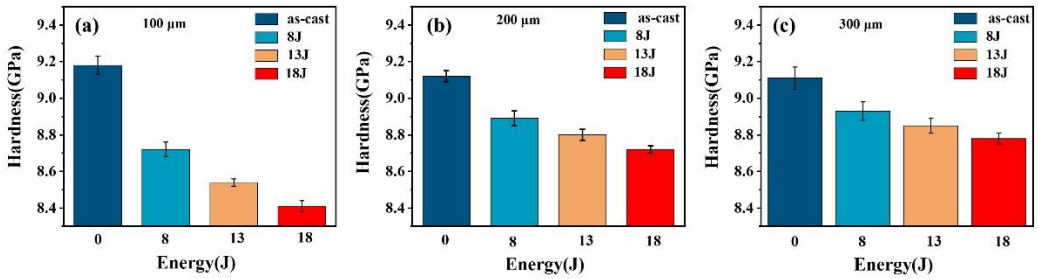

Fig. 6. Nano-hardness values at different depths along the LSP direction of the as-cast and LSP-treated $Ti_{40}Zr_{25}Ni_3Cu_{12}Be_{20}$ bulk metallic glass samples with different laser-beam energies: 100 μm, (b) 200 μm, and (c) 300 μm.To study the mechanical properties of LSP-treated BMGs samples along the LSP depth direction, the nano-hardness measurements of the present studied BMGs were performed at different depths, and the corresponding values were plotted in Fig. 6 (100 μm [Fig. 6(a)], 200 μm [Fig. 6(b)], and 300 μm [Fig. 6(c)]. As seen, the nano-hardness of LSP-treated samples shows a decreasing trend [Fig. 6(a),

from 9.18 GPa to 8.41 GPa, Fig. 6(b), from 9.12 GPa to 8.72 GPa, Fig. 6(c), from 9.11 GPa to 8.78 GPa, for 100 μm, 200 μm, and 300 μm depths along the LSP direction, respectively], compared to as-cast samples. The results indicated that the LSP treatment induces a softening effect in $Ti_{40}Zr_{25}Ni_3Cu_{12}Be_{20}$ BMG samples. Numerous studies have proved that the increase in the free-volume content can cause a decrease in nano-hardness, leading to a softening effect [35, 36]. Due to the high-pressure shock wave (surpasses the elastic limit of $Ti_{40}Zr_{25}Ni_3Cu_{12}Be_{20}$ BMGs samples) generated by LSP, the surface of the matrix undergoes deformation. The internal stress induced by the shock-wave pressure makes atoms deviate more easily from the perfect close-packed structure, and these atoms are forced into the adjacent hole, facilitating the generation of the excess free volume. The LSP-treated $Ti_{40}Zr_{25}Ni_3Cu_{12}Be_{20}$ BMGs samples exhibit lower local order extents, i.e., more free-volume content, compared with the as-cast sample (See Fig. 4). The loose arrangement of atoms at the free volume results in lower deformation resistance and thus lower nano-hardness of the LSP-treated samples (See Fig. 6). Additionally, the nano-hardness of LSP-treated samples (8J) appears an upward trend with increasing the depth along the LSP direction (8.72 GPa, 8.89 GPa, and 8.94 GPa, for 100 μm, 200 μm, and 300 μm, respectively), gradually approaching the nano-hardness of the matrix (9.11 GPa). This trend can be attributed to the presence of a gradient effect in the LSP-treated samples along the LSP direction, where the structure changes induced by LSP become progressively smaller and tend to approach the as-cast state [See Fig. 5(d)-5(f), with fewer shear bands]. Therefore, the structures of LSP-treated BMG samples along the LSP direction becomes denser with less free volume, resulting in an increase in the nano-hardness value. Moreover, increasing the energy further causes a decrease in the nano-hardness of LSP-treated samples [See Fig. 6(a), 8.72 GPa, 8.53GPa, 8.41GPa, for 8J, 13J and18J, respectively]. The maximum shock-wave pressure increases with increasing the energy (2.76 GPa, 3.52 GPa, and 4.14 GPa, for 8J, 13J, and18J, respectively), further decreasing the energy barrier in the BMG system. More atoms are forced into the adjacent hole, generating more free volume contents and thus, causing a lower local order extent (See Figs. 4 and 5). Figure 7

schematically illustrates the evolution of the structure for the as-cast BMG (Fig. 7a) and LSP-treated BMGs with different laser beam energies (Figs. 7b, 7c, and 7d). The variation in the number of red dotted circles [Fig. 7] indicates changes in free volume contents within the studied BMG samples LSP-treated with different laser beam energies. Due to the continuous increase in the free volume content, the deformation resistance of LSP-treated samples further decreases, leading to a gradual reduction in nano-hardness, as the laser--beam energy increases.

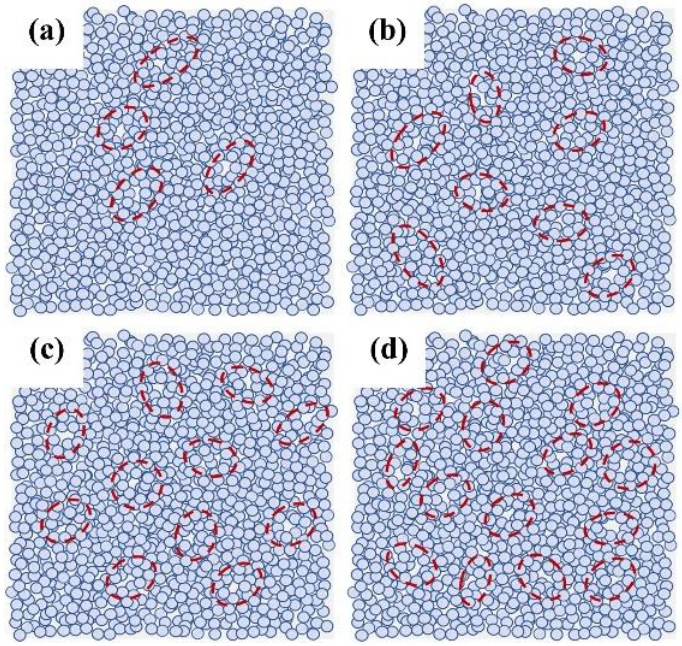

Fig. 7. Structure diagrams of the as-cast $Ti_{40}Zr_{25}Ni_3Cu_{12}Be_{20}$ BMG (a) and LSP-treated BMG samples with different laser beam energies of (b) 8J, (c) 13J, and (d) 18J.

4. Conclusion

In this paper, the effect of different laser-beam energies on the structures and mechanical properties of $Ti_{40}Zr_{25}Ni_3Cu_{12}Be_{20}$ BMGs is investigated, using structural observations, numerical simulations and nanoindentation tests. The main conclusions can be drawn as follows:

(1) Plastic deformation of the studied $Ti_{40}Zr_{25}Ni_3Cu_{12}Be_{20}$ BMGs samples occurs under the treatment of LSP. The value of the residual stress inside the matrix is positively correlated with the laser-beam energy but is negatively correlated with the depth along the LSP direction. Besides, the LSP-treated samples remain as an

amorphous structure at different laser-beam energies (8J, 13J, and 18J).

(2) As the laser-beam energy increases, the increase in the shock-wave pressure causes a reduction in the local order extent and thus, an increase in the free-volume contents of LSP-treated $Ti_{40}Zr_{25}Ni_3Cu_{12}Be_{20}$ BMGs samples. The higher free volume content further promotes the formation of more shear bands within the matrix, causing a decrease in nano-hardness.

(3) There exists a gradient effect along the LSP direction inside the sample, where the softening effect of LSP gradually decays with increasing the depth. This trend results in an increase in the nano-hardness along the LSP direction.

Acknowledgements

The authors would like to acknowledge the financial support from the Interdisciplinary Research Foundation of HIT under Grant No. IR2021201, the CGN-HIT Advanced Nuclear and New Energy Research Institute (Grant No. CGN-HIT202209), and the National Natural Science Foundation of China under Grant Nos. 52171154, 51827801, and 52071118. PKL very much appreciates the support from the National Science Foundation (DMR – 1611180, 1809640, and 2226508).

References

[1] S.S. Jiang, K.F. Gan, Y.J. Huang, P. Xue, Z.L. Ning, J.F. Sun, A.H.W. Ngan, Stochastic deformation and shear transformation zones of the glassy matrix in CuZr-based metallic-glass composites, Int. J. Plast. 125 (2020) 52-62. https://doi.org/10.1016/j.ijplas.2019.09.005.

[2] W.L. Johnson, K. Samwer, A universal criterion for plastic yielding of metallic glasses with a $(T/T_g)^{2/3}$ temperature dependence, Phys. Rev. Lett. 95 (2005) 195501-195504. https://doi.org/10.1103/PhysRevLett.95.195501.

[3] L. Liao, R. Gao, Z.H. Yang, S.T. Wu, Q. Wan, A study on the wear and corrosion resistance of high-entropy alloy treated with laser shock peening and PVD coating, Surf. Coat. Technol. 437 (2022) 128281. https://doi.org/10.1016/j.surfcoat.2022.128281.

[4] D. Pan, A. Inoue, T. Sakurai, M.W. Chen, Experimental characterization of shear transformation zones for plastic flow of bulk metallic glasses, Proc. Natl. Acad. Sci. U.S.A. 105 (2008) 14769-14772. https://doi.org/10.1073/pnas.0806051105.

[5] M. Zhang, Y.J. Wang, L.H. Dai, Bridging shear transformation zone to the atomic structure of amorphous solids, J. Non-Cryst. Solids. 410 (2015) 100-105. https://doi.org/10.1016/j.jnoncrysol.2014.12.020.

[6] A. Ermakova, J. Braithwaite, J. Razavi, S. Ganguly, F. Berto, A. Mehmanparast, The influence of laser shock peening on corrosion-fatigue behaviour of wire arc additively manufactured components, Surf. Coat. Technol. 456 (2023) 129262. https://doi.org/10.1016/j.surfcoat.2023.129262.

[7] E. Maleki, S. Bagherifard, O. Unal, A. Jam, S. Shao, M. Guagliano, N. Shamsaei, Superior effects of hybrid laser shock peening and ultrasonic nanocrystalline surface modification on fatigue behavior of additive manufactured $AlSi_{10}Mg$, Surf. Coat. Technol. 463 (2023) 129512. https://doi.org/10.1016/j.surfcoat.2023.129512.

[8] L. Zhang, S. Su, W. Fu, J. Sun, Z. Ning, A.H.W. Ngan, Y. Huang, Strain-induced structural evolution of interphase interfaces in CuZr-based metallic-glass composite reinforced by B2 crystalline phase, Composites, Part B. 258 (2023) 110698. https://doi.org/10.1016/j.compositesb.2023.110698.

[9] S.S. Jiang, Y.J. Huang, F.F. Wu, P. Xue, J.F. Sun, A CuZr-based bulk metallic glass composite with excellent mechanical properties by optimizing microstructure, J. Non-Cryst. Solids. 483 (2018) 94-98. https://doi.org/10.1016/j.jnoncrysol.2018.01.006.

[10] W.H. Jiang, F.X. Liu, Y.D. Wang, H.F. Zhang, H. Choo, P.K. Liaw, Comparison of mechanical behavior between bulk and ribbon Cu-based metallic glasses, Mater. Sci. Eng. A 430 (2006) 350-354. https://doi.org/10.1016/j.msea.2006.05.042.

[11] Y. Zhang, W.H. Wang, A.L. Greer, Making metallic glasses plastic by control of residual stress, Nat. Mater. 5 (2006) 857-860. https://doi.org/10.1038/nmat1758.

[12] W.F. Ma, H.C. Kou, J.S. Li, H. Chang, L. Zhou, Effect of strain rate on compressive behavior of Ti-based bulk metallic glass at room temperature, J. Alloys Compd. 472 (2009) 214-218. https://doi.org/10.1016/j.jallcom.2008.04.043.

[13] K.K. Song, S. Pauly, Y. Zhang, S. Scudino, P. Gargarella, K.B. Surreddi, U. Kuhn, J. Eckert, Significant tensile ductility induced by cold rolling in $Cu_{47.5}Zr_{47.5}Al_5$ bulk

metallic glass, Intermetallics 19 (2011) 1394-1398. https://doi.org/10.1016/j.intermet.2011.05.001.
[14] Y. Li, Y. Wei, X. Yi, K. Zhang, B. Wei, Abnormal change in dynamic mechanical behavior of metallic glass by laser shock peening, Opt. Laser Technol. 138 (2021) 106875. https://doi.org/10.1016/j.optlastec.2020.106875.
[15] Z.H. Mahmoud, H. Barazandeh, S.M. Mostafavi, K. Ershov, A. Goncharov, A.S. Kuznetsov, O.D. Kravchenko, Y. Zhu, Identification of rejuvenation and relaxation regions in a Zr-based metallic glass induced by laser shock peening, J. Mater. Res. Technol. 11 (2021) 2015-2020. https://doi.org/10.1016/j.jmrt.2021.02.025.
[16] S. Qi, H. Bao, Y. Shen, Numerical investigation on spall fracture in a metallic material caused by laser shock peening, Mater. Today Commun. 33 (2022) 104343. https://doi.org/10.1016/j.mtcomm.2022.104343.
[17] X. Zhang, Y.e. Ma, M. Yang, C. Zhou, N. Fu, W. Huang, Z. Wang, A comprehensive review of fatigue behavior of laser shock peened metallic materials, Theor. Appl. Fract. Mech. 122 (2022) 103642. https://doi.org/10.1016/j.tafmec.2022.103642.
[18] C. Zhang, Y. Dong, C. Ye, Recent developments and novel applications of laser shock peening: a review, Adv. Eng. Mater. 23 (2021) 2001216. https://doi.org/10.1002/adem.202001216.
[19] Y. Li, Z. Wang, Y. Wei, T. Chen, C. Zhang, Y. Huan, K. Zhang, B. Wei, The evolution of micromechanical properties for Zr-based metallic glass induced by laser shock peening, Front. Mater. 8 (2021) 802972. https://doi.org/10.3389/fmats.2021.802973.
[20] J. Wang, Y. Gao, X. Wei, Investigations of the effects of combination treatments on the fretting fatigue resistance of GH4169 superalloy at an elevated temperature, Surf. Coat. Technol. 426 (2021) 127758. https://doi.org/10.1016/j.surfcoat.2021.127758.
[21] J. Fu, Y. Zhu, C. Zheng, R. Liu, Z. Ji, Effect of laser shock peening on mechanical properties of Zr-based bulk metallic glass, Appl. Surf. Sci. 313 (2014) 692-697. https://doi.org/10.1016/j.apsusc.2014.06.056.
[22] Y. Cao, X. Xie, J. Antonaglia, B. Winiarski, G. Wang, Y.C. Shin, P.J. Withers, K.A. Dahmen, P.K. Liaw, Laser shock peening on Zr-based bulk metallic glass and its effect on plasticity: experiment and modeling, Sci. Rep. 5 (2015) 10789. https://doi.org/10.1038/srep10789.
[23] S. Li, T. Yamaguchi, High-temperature oxidation performance of laser-cladded amorphous TiNiSiCrCoAl high-entropy alloy coating on Ti-6Al-4V surface, Surf. Coat. Technol. 433 (2022) 128123. https://doi.org/10.1016/j.surfcoat.2022.128123.
[24] W.J. Fu, Y.J. Huang, J.F. Sun, A.H.W. Ngan, Strengthening $CrFeCoNiMn_{0.75}Cu_{0.25}$ high entropy alloy via laser shock peening, Int. J. Plast. 154 (2022) https://doi.org/10.1016/j.ijplas.2022.103296.
[25] Y.H. Zhu, J. Fu, C. Zheng, Z. Ji, Influence of laser shock peening on morphology and mechanical property of Zr-based bulk metallic glass, Opt. Laser Eng. 74 (2015) 75-79. https://doi.org/10.1016/j.optlaseng.2015.05.012.
[26] G.Y. Fan, J.M. Cowley, Autocorrelation analysis of high-resolution electron-micrographs of near-form thin-films, Ultramicroscopy 17 (1985) 345-355. https://doi.org/10.1016/0304-3991(85)90201-3.

[27] J. Fu, Y. Zhu, C. Zherig, R. Liu, Z. Ji, Evaluate the effect of laser shock peening on plasticity of Zr-based bulk metallic glass, Opt. Laser Technol. 73 (2015) 94-100. https://doi.org/10.1016/j.optlastec.2015.04.009.
[28] R. Fabbro, J. Fournier, P. Ballard, D. Devaux, J. Virmont, Physical study of laser-produced plasma in confined geometry, J. Appl. Phys. 68 (1990) 775-784. https://doi.org/10.1063/1.346783.
[29] W.W. Zhang, Y.L. Yao, Micro scale laser shock processing of metallic components, J. Manuf. Sci. E-T ASME. 124 (2002) 369-378. https://doi.org/10.1115/1.1445149.
[30] D.J. Lacks, M.J. Osborne, Energy landscape picture of overaging and rejuvenation in a sheared glass, Phys. Rev. Lett. 93 (2004) 255501. https://doi.org/10.1103/PhysRevLett.93.255501.
[31] L.Z. Zhao, R.J. Xue, Y.Z. Li, W.H. Wang, H.Y. Bai, Revealing localized plastic flow in apparent elastic region before yielding in metallic glasses, J. Appl. Phys. 118 (2015) 244901. https://doi.org/10.1063/1.4938567.
[32] K. Tao, F.C. Li, Y.H. Liu, E. Pineda, K.K. Song, J.C. Qiao, Unraveling the microstructural heterogeneity and plasticity of $Zr_{50}Cu_{40}Al_{10}$ bulk metallic glass by nanoindentation, Int. J. Plast. 154 (2022) 103305. https://doi.org/10.1016/j.ijplas.2022.103305.
[33] A.S. Argon, Plastic deformation in metallic glasses, Acta Mater. 27 (1979) 47-58. https://doi.org/10.1016/0001-6160(79)90055-5.
[34] A. Bolshakov, G.M. Pharr, Influences of pileup on the measurement of mechanical properties by load and depth sensing indentation techniques, J. Mater. Res. 13 (1998) 1049-1058. https://doi.org/10.1557/jmr.1998.0146.
[35] J. Tan, Y. Zhang, B.A. Sun, M. Stoica, C.J. Li, K.K. Song, U. Kuhn, F.S. Pan, J. Eckert, Correlation between internal states and plasticity in bulk metallic glass, Appl. Phys. Lett. 98 (2011) https://doi.org/10.1063/1.3580774.
[36] L.Y. Chen, A.D. Setyawan, H. Kato, A. Inoue, G.Q. Zhang, J. Saida, X.D. Wang, Q.P. Cao, J.Z. Jiang, Free-volume-induced enhancement of plasticity in a monolithic bulk metallic glass at room temperature, Scr. Mater. 59 (2008) 75-78. https://doi.org/10.1016/j.scriptamat.2008.02.025.